

Secondary bifurcations and transverse standing-wave patterns in anisotropic microcavity lasers close to the first laser threshold

I. V. Babushkin and N. A. Loiko*

Institute of Physics, Academy of Sciences of Belarus, Scaryna Prospekt 70, 220072 Minsk, Belarus

T. Ackemann†

Institute for Applied Physics, University of Münster, Corrensstrasse 2-4, 48149 Münster, Germany

(Received 14 September 2002; published 29 January 2003)

It is well known that in a laser—in the limit of an infinite extent of the transverse aperture—traveling tilted waves are excited at the laser threshold for positive detuning between the frequency of the gain maximum of the active medium and the cavity frequency [Phys. Rev. A **45**, 8129 (1992)]. However, a transverse standing wave is unstable. In this paper, it is shown that in anisotropic lasers there can be a chain of secondary bifurcations very close to threshold, which stabilizes the standing wave and then destabilizes it again through a supercritical Hopf bifurcation. The parameter dependence of these bifurcations is discussed. The investigations are motivated by interest in pattern formation in vertical-cavity surface-emitting lasers in which the rotational symmetry is broken due to the dependence of the reflectance of the Bragg reflectors on the polarization vector of the field. The applicability of the results to other class-*B* lasers is discussed.

DOI: 10.1103/PhysRevA.67.013813

PACS number(s): 42.60.Jf, 42.65.Sf

I. INTRODUCTION

Since their appearance [1], vertical-cavity surface-emitting lasers (VCSELs) have attracted a great deal of attention because of many new properties, such as the small size of the cavity, the possibility of single longitudinal mode operation, polarization isotropy, low threshold, and so on [2].

In the past few years, VCSELs with a large transverse aperture were created, providing an increase of output power [3]. However, it is known that with increasing transverse size, higher-order transverse modes might be generated, making the output inhomogeneous and filamented. The shape of the resulting pattern depends strongly on the device size. For a comparatively small size, the transverse structure is strongly determined by the transverse boundary conditions. The main method of theoretical investigation of such structures is a decomposition into transverse modes of the empty cavity, which are defined mainly by the boundary conditions [4]. When the size of the aperture is increased, the structure of the transverse pattern is determined by nonlinear interactions of transverse Fourier modes (tilted waves) of the laser field [5–7]. First experimental studies of such VCSELs show that—for rather homogeneous pumping—transverse standing waves often appear near the first laser threshold in both rectangular [8] and circular devices [9].

An often used theoretical approach to describe pattern formation is to decompose the field into transverse Fourier harmonics that have the form $A(t, z)\exp(ik_x x + ik_y y)$ [where $\mathbf{x}_t = (x, y)$ is a coordinate in the transverse plane and $\mathbf{k}_t = (k_x, k_y)$ is a transverse wave vector]. Under certain conditions, a limited family of “critical” Fourier modes has the

lowest threshold of generation, and it is possible to find order-parameter equations for these Fourier modes, describing their spatially temporal evolution on slow scales [10,11]. The simplest theory, using the above-mentioned decomposition, is based on the Maxwell-Bloch equations for two-level media and the field, averaged over the whole cavity. It predicts the stability of a traveling transverse wave (TW) at the laser threshold, whereas a standing wave (SW) is unstable for both class-*A* [10] and class-*B* [11] lasers. However, for semiconductor lasers, TWs appear also to be unstable with respect to long-wavelength transverse perturbations due to phase-amplitude coupling governed by the so-called α factor. This leads to spatiotemporal chaos [12], since all critical spatial Fourier modes are destabilized. The family of such modes forms a circle in two-dimensional (2D) transverse Fourier space, because the threshold depends only on $|\mathbf{k}_t|^2 = k_x^2 + k_y^2$ [11,12]. In contrast, in a VCSEL the rotational symmetry is broken due to the properties of the Bragg reflectors enclosing the cavity [13]. In this case, only two tilted waves with certain wave vectors $\mathbf{k}_{th} = (k_{x,th}, k_{y,th})$ and $-\mathbf{k}_{th}$ appear at the laser threshold.

In this paper, we obtain the appropriate order-parameter equations under conditions of symmetry breaking in $\mathbf{k}_t = (k_x, k_y)$ space. For the very close vicinity of threshold, these order-parameter equations constitute a system of Ginsburg-Landau (GL) equations describing the complex amplitudes of two excited modes. Using these equations, we show that a SW is unstable at the very threshold, whereas a TW might be either stable or unstable with respect to spatial long-wavelength perturbations. Its stability depends on the α factor. If the TW is unstable, irregular spatiotemporal dynamics of the amplitude of the TW is obtained. This situation coincides with the one analyzed in [11,12].

However, the system of GL equations of any order is degenerate because it possesses an additional symmetry, which is not present in the original equations [14]. We show here

*Email address: nloiko@dragon.bas-net.by; FAX: +375 172 840879.

†FAX: +49-251-83-33513.

that, if the influence of dynamics of the spatial variations of the carrier population is taken into account, this additional symmetry disappears, giving rise to the following sequence of secondary bifurcations with increasing value of the pump parameter: destabilization of TW, stabilization of SW, Hopf bifurcation of SW. The last bifurcation results in a stripe pattern, in which the amplitudes of the constituent modes oscillate in time.

This paper is organized as follows. In the second section, we give the basic equations describing a laser with transverse anisotropy. Analysis of the GL equations is presented in Sec. III. It is followed by equations describing spatial variations of the carrier population due to two-spatial-mode interaction (which we call “the two-mode approximation”) in Sec. IV. In the final section, we discuss the main results and point out possible prospects of this work.

II. THE BASIC EQUATIONS

In the following, we will consider a model for a single-longitudinal mode microcavity laser filled with an active medium with a Lorentzian line shape. Specifically, the model was introduced in [13,15] as a model for a VCSEL taking into account anisotropy in \mathbf{k}_t space. The analysis is based on a system of partial differential equations describing the behavior of the complex field profile $e(t, x, y)$ and population inversion profile $d(t, x, y)$. $e(t, x, y)$ is slowly varying in time since a carrier wave of the form $\exp(-i\omega_0 t - ik_0 z)$ was split off (ω_0 longitudinal resonance of cavity, k_0 corresponding wave number). Real devices emit usually at threshold in a linearly polarized mode with a well-defined polarization due to small gain and loss anisotropies caused by dichroism and birefringence [16–19]. The preference for a defined linear polarization state close to threshold was recently confirmed also in large aperture devices [8,9]. Hence only one polarization component of the field is taken into account, for simplicity. Under these assumptions we have [13,15]

$$\dot{e} = -\hat{L}e + \hat{G}(de), \quad (1)$$

$$\dot{d} = -d + \mu - \text{Im}[(i - \alpha)e^* \hat{L}(de)], \quad (2)$$

where κ is the field decay rate. All the operators \hat{L} , \hat{G} , and $\hat{\mathcal{L}}$ are functions in \mathbf{k}_t space. Thus, for example, for any function $f(\mathbf{x}_t)$, we have $\hat{L}(f(\mathbf{x}_t)) = [\hat{\mathcal{F}}^{-1}(L(\mathbf{k}_t)\hat{\mathcal{F}}(f)(\mathbf{k}_t))](\mathbf{x}_t)$, where $[\hat{\mathcal{F}}(f)(\mathbf{k}_t)](\mathbf{k}_t) = \int_{-\infty}^{\infty} f(\mathbf{x}_t) \exp(-i\mathbf{k}_t \cdot \mathbf{x}_t) dk_x dk_y$ is the Fourier transform and $\hat{\mathcal{F}}^{-1}$ is the inverse one.

The operator $\hat{L} = \kappa(\hat{F}_L/F_{L0} + i\alpha)$ describes diffraction and losses in the cavity. It contains the operators of the field propagation through the bottom (\hat{F}_1) and the top (\hat{F}_2) parts of the cavity [$\hat{F}_L = 1 - \hat{F}_1\hat{F}_2$ and $F_{L0} = F(\mathbf{k}_t = \mathbf{0})$]. The modal gain is described by the operator $\hat{G} = \kappa(1 + i\alpha)(\hat{F}_G/F_{G0})\hat{\mathcal{L}}$ [where $\hat{F}_G = 1 + \hat{F}_1 + \hat{F}_2 + \hat{F}_1\hat{F}_2$ and $F_{G0} = F_G(\mathbf{k}_t = 0)$]. The operator $\hat{\mathcal{L}} \rightarrow L(\mathbf{k}_t) = 1/[1 + [\delta - \Omega(\mathbf{k}_t)]^2/\gamma^2]$ describes the Lorentzian profile of the gain line (here $\delta = \omega_g - \omega_c$ is the detuning of the peak of

the gain spectrum from the cavity resonance, γ determines a linewidth of the gain, and $\Omega(\mathbf{k}_t)$ will be described in the next paragraph).

The propagation operator

$$\hat{F}_{i \rightarrow}^{\mathcal{F}} F_i(\mathbf{k}_t) = T_i(\mathbf{k}_t) R_i(\mathbf{k}_t) \exp[i\Omega(\mathbf{k}_t)\tau_i]$$

is calculated in paraxial approximation and includes the reflection from the Bragg reflector $R_i(\mathbf{k}_t)$, the propagation in the spacer layer $T_i(\mathbf{k}_t) \sim \exp(iL_i\mathbf{k}_t/k)$, and an additional phase shift $\exp[i\Omega(\mathbf{k}_t)\tau_i]$. τ_i is the time the light needs to pass through part i of the resonator. This phase shift arises because the frequency of the lasing field will in general differ from the carrier frequency assumed in taking the slowly varying envelope approximation by a frequency shift $\Omega(\mathbf{k}_t)$ for the mode \mathbf{k}_t [13,15]. $\Omega(\mathbf{k}_t)$ is evaluated from the threshold condition (see [13,15]). It turns out that it almost coincides with the resonant frequency of each Fourier component \mathbf{k}_t in the empty cavity.

The complex reflection coefficients of the Bragg reflectors are evaluated by matrix propagation methods and are given in detail elsewhere [25,26]. It is important to note that the polarizations of the field are mixed during the reflection, and therefore the reflection operator constitutes a matrix,

$$R_i(\mathbf{k}_t) = \begin{pmatrix} R_i^{(11)}(\mathbf{k}_t) & R_i^{(12)}(\mathbf{k}_t) \\ R_i^{(21)}(\mathbf{k}_t) & R_i^{(22)}(\mathbf{k}_t) \end{pmatrix}. \quad (3)$$

Under the assumption of a single polarization mode we have $R_i(\mathbf{k}_t) = R_i^{(11)}(\mathbf{k}_t)$. The degree of mixing depends not only on the angle of incidence of the light component onto the Bragg mirror (which is proportional to $|\mathbf{k}_t|$), but also on the angle between the polarization vector and the transverse wave vector. Hence it depends on the direction of \mathbf{k}_t . This anisotropy of the Bragg reflector is shown in Figs. 1(a) and 1(b) for an x -polarized field.

As a consequence of this symmetry breaking, also the first laser threshold will depend on the transverse wave vector [see Figs. 1(c) and 1(d)], whereas in an isotropic laser a whole ring of wave vectors with a defined value of $|\mathbf{k}_{\text{th}}|$ (and arbitrary angle) becomes linearly unstable at threshold, if the detuning of the peak of the gain spectrum from the cavity resonance, $\delta = \omega_g - \omega_c$, is positive [5–7]. Specifically, it was shown earlier by some of the authors that the lowest threshold belongs to exactly two transverse Fourier modes of the field, characterized by transverse wave vectors \mathbf{k}_{th} and $-\mathbf{k}_{\text{th}}$ [13,15] [see Figs. 1(c) and 1(d)].

III. GINSBURG-LANDAU EQUATIONS

In the following, we are deriving a system of two coupled equations, describing the behavior of these two field modes. However, we have to remember that the neglect of the dynamics of the carrier density—and hence the applicability of these equations—is limited to a very tiny range of pump levels above threshold due to the stiffness of the class-B laser equations [11].

To obtain the equations by a weakly nonlinear analysis, a multiple-scale expansion method is used [10]. We introduce slow scales in space and time by

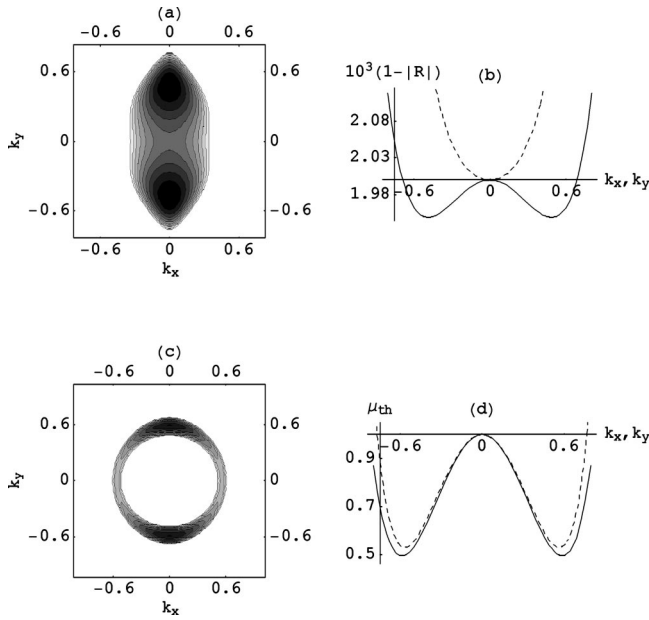


FIG. 1. The dependence of the reflection of a Bragg reflector $|R(\mathbf{k}_r)|$ [(a),(b)] and threshold current μ_{th} [(c),(d)] on $\mathbf{k}_r = (k_x, k_y)$ for an x -polarized field. (b) is a cross section of (a) with $k_x=0$ (solid line) and $k_y=0$ (dashed line). (d) is a cross section of (c) with $k_x=0$ (solid line) and $k_y=0$ (dashed line). Values of k_x, k_y are given in arbitrary units. Parameters are $\alpha=3$, $\kappa=285.1$, $\delta=0.99\gamma$, and $\gamma=10^{11}\text{s}^{-1}$; the other parameters of the cavity and the Bragg mirrors are taken from [9]. $\mu_{\text{th}}(\mathbf{k}_r)$ is normalized such that $\mu_{\text{th}}(0)=1$.

$$t \rightarrow \sqrt{\epsilon}T_1 + \epsilon T_2 + \dots,$$

$$(x, y) \rightarrow \sqrt{\epsilon}(X_1, Y_1) + \epsilon(X_2, Y_2) + \dots, \quad (4)$$

where $\epsilon = \mu - \mu_{\text{th}}$ is the deviation of the pump parameter from its threshold value μ_{th} . It should be noted that the scaling factors for both coordinates x and y are the same because of the anisotropy of the system, whereas in the case of isotropic mirrors a scaling like $(x, y) \rightarrow (\sqrt{\epsilon}X_1, \epsilon Y_1) + (\epsilon X_2, \epsilon^2 Y_2) + \dots$ is selected. This situation is quite general for anisotropic systems [20].

To simplify the operators $\hat{L}, \hat{G}, \hat{L}$, we note that near threshold the field has the form

$$e(t, \mathbf{x}_r) = e^{(+)}(t, \mathbf{x}_r) \exp(i\mathbf{k}_r \cdot \mathbf{x}_r) + e^{(-)}(t, \mathbf{x}_r) \exp(-i\mathbf{k}_r \cdot \mathbf{x}_r),$$

where the amplitudes $e^{(+)}, e^{(-)}$ are slowly varying functions in space and time. Then we decompose the operators $\hat{A} = \hat{L}, \hat{G}$ or \hat{L} into two parts, each acting on the corresponding amplitude of the field,

$$\begin{aligned} \hat{A}[e^{(+)}(t, \mathbf{x}_r) \exp(i\mathbf{k}_r \cdot \mathbf{x}_r) + e^{(-)}(t, \mathbf{x}_r) \exp(-i\mathbf{k}_r \cdot \mathbf{x}_r)] \\ = \exp(i\mathbf{k}_r \cdot \mathbf{x}_r) [\hat{A}^{(+)} e^{(+)}(t, \mathbf{x}_r)] \\ + \exp(-i\mathbf{k}_r \cdot \mathbf{x}_r) [\hat{A}^{(-)} e^{(-)}(t, \mathbf{x}_r)]. \end{aligned} \quad (5)$$

Because $e^{(+)}, e^{(-)}$ are slowly varying in space, the corresponding Fourier image $\tilde{e}^{(\pm)}(t, \mathbf{k}_r) = \mathcal{F}e^{(\pm)}(t, \mathbf{x}_r)$ is a wave

packet localized near $\mathbf{k}_r = \mathbf{0}$. Therefore, we can decompose the operators \hat{A} , which are functions in \mathbf{k}_r space, into series near $\mathbf{q} = \mathbf{0}$ [$\mathbf{q} = \pm(\mathbf{k}_r - \mathbf{k}_{\text{th}})$],

$$\begin{aligned} \hat{A}^{(\pm)} \xrightarrow{\mathcal{F}} A^{(\pm)}(\mathbf{q}) \approx (A_\alpha^{(\pm)} + A_\beta^{(\pm)(i)} q_i + A_\gamma^{(\pm)(ij)} q_i q_j) \\ \xrightarrow{\mathcal{F}^{-1}} \left(A_\alpha^{(\pm)} - iA_\beta^{(\pm)(i)} \frac{\partial}{\partial x_i} - A_\gamma^{(\pm)(ij)} \frac{\partial^2}{\partial x_i \partial x_j} \right), \end{aligned} \quad (6)$$

with coefficients $A_\alpha^{(\pm)}, A_\beta^{(\pm)(i)}, A_\gamma^{(\pm)(ij)}$ defined as

$$A_\alpha^{(\pm)} = A(\pm \mathbf{k}_{\text{th}}), \quad (7)$$

$$A_\beta^{(\pm)(i)} = \frac{\partial A(\pm \mathbf{k}_{\text{th}})}{\partial k_i}, \quad (8)$$

$$A_\gamma^{(\pm)(ij)} = \frac{1}{2} \frac{\partial^2 A(\pm \mathbf{k}_{\text{th}})}{\partial k_i \partial k_j}, \quad (9)$$

and the Einstein summation rule in Eq. (6) is assumed over repeated indexes $i=(1,2)$ (here we identify q_1, q_2 with q_x, q_y and x_1, x_2 with x, y to simplify the expressions). In Eq. (9), we can restrict the expansion to derivatives up to the second order of q_i because of the anisotropy of the system [20]. In the case of isotropic mirrors, the derivatives in q_y are zero up to the fourth order, and hence higher derivatives than second order need to be taken into account. In this sense the case of anisotropic Bragg mirrors is more simple to treat analytically than the isotropic case. In addition, it is known that the reflection operator $R_i(\mathbf{k}_r)$ is invariant under inversion $\mathbf{k}_r \rightarrow -\mathbf{k}_r$, and the same can be said about the transition operator $T_i(\mathbf{k}_r)$. Therefore, $A_\alpha^{(+)} = A_\alpha^{(-)} \equiv A_\alpha$, $A_\beta^{(+)(i)} = -A_\beta^{(-)(i)} \equiv A_\beta^{(i)}$, and $A_\gamma^{(+)(ij)} = A_\gamma^{(-)(ij)} \equiv A_\gamma^{(ij)}$.

Applying Eqs. (4)–(9) to Eqs. (1) and (2), and comparing coefficients of equal degrees of ϵ , we will obtain a system of two coupled complex Ginsburg-Landau equations,

$$\begin{aligned} \left(-\frac{\partial}{\partial t} + \sum_{i=1}^2 a_i^{(\pm)} \frac{\partial}{\partial x_i} + \sum_{i=1}^2 \sum_{j<i} a_{ij}^{(\pm)} \frac{\partial^2}{\partial x_i \partial x_j} + a_0^{(\pm)} \right. \\ \left. + p_{\text{NL}_2}(e^{(\pm)}, e^{(\mp)}) + p_{\text{NL}_4}(e^{(\pm)}, e^{(\mp)}) \right) e^{(\pm)} = 0, \end{aligned} \quad (10)$$

where

$$a_0^{(\pm)} = \mu G_\alpha^{(\pm)} - L_\alpha^{(\pm)}, \quad a_i^{(\pm)} = -i(\mu_{\text{th}} G_\beta^{(\pm)(i)} - L_\beta^{(\pm)(i)}),$$

$$a_{ij}^{(\pm)} = -\mu_{\text{th}} G_\gamma^{(\pm)(ij)} + L_\gamma^{(\pm)(ij)},$$

and

$$\mu_{\text{th}} = \text{Re}(L_\alpha) / \text{Re}(G_\alpha)$$

is the threshold pump level.

The nonlinear parts of second order $p_{NL_2}(a,b) = -\mu G_\alpha \mathcal{L}_\alpha(|a|^2 + 2|b|^2)$ and of fourth order $p_{NL_4}(a,b) = \frac{1}{2}\mu G_\alpha \mathcal{L}_\alpha^2[2|a|^4 + (5+i\alpha)|b|^4 + (11-i\alpha)|a|^2|b|^2]$ depend only on the modulus of their arguments. Hence, Eqs. (10) have the important property of possessing a two-parametric family of symmetries, corresponding to a phase shift of each field e_+, e_- separately. It is easy to see that the original system (1) and (2) does not have such a symmetry. Another important point to note is that the terms p_{NL_2} and p_{NL_4} have different signs. The lowest-order nonlinear term p_{NL_2} restricts the growth of perturbations growing due to the driving term $a_0^{(\pm)}$ term above threshold, whereas the second nonlinear term p_{NL_4} destabilizes the system still more.

The system (10) has two families of solutions with constant amplitude. The first one is TW, with

$$|e_\mp|^2 = 0, \quad |e_\pm|^2 = \frac{\beta}{2\mathcal{L}_\alpha}, \quad (11)$$

where $\beta = 1 - \sqrt{-3 + 4\mu_{th}/\mu}$, and the second is SW with

$$|e_\pm|^2 = |e_\mp|^2 = \frac{\beta}{6\mathcal{L}_\alpha}. \quad (12)$$

The characteristic polynomial describing the stability of Eq. (10) has four roots. At $\mathbf{q} = \mathbf{0}$ they determine the stability with respect to perturbations with the same wave vector $\pm \mathbf{k}_{th}$. Two of these have zero real parts for both SW and TW solutions at $\mathbf{q} = \mathbf{0}$. Close to threshold, the other two roots are given up to the second order of ϵ by the expression

$$\lambda_1 \approx -\frac{\text{Re}(L_\alpha)}{2\mu_{th}}\epsilon + \frac{\text{Re}(L_\alpha)}{2\mu_{th}^2}\epsilon^2, \quad (13)$$

$$\lambda_2 \approx -\frac{1}{2}\text{Re}(G_\alpha)\epsilon + \frac{\text{Re}(G_\alpha) - \alpha \text{Im}(G_\alpha)}{4\mu_{th}}\epsilon^2 \quad (14)$$

for the TW solution, and

$$\lambda_1 \approx -\frac{1}{2}\text{Re}(G_\alpha)\epsilon + \frac{\text{Re}(G_\alpha)}{2\mu_{th}}\epsilon^2, \quad (15)$$

$$\lambda_2 \approx \frac{1}{6}\text{Re}(G_\alpha)\epsilon + \frac{1}{18}\frac{\text{Im}(G_\alpha)\alpha}{\mu_{th}}\epsilon^2 \quad (16)$$

for the SW solution. The term that is of linear order in ϵ describes the behavior of the GL equations with the fourth-order term p_{NL_4} omitted. If only this linear term is taken into account, there are no secondary bifurcations above threshold. Including the more precise expression of order ϵ^2 , it is obtained that TW loses its stability at the point $\epsilon \approx \mu_{th} \sim 1$. It is worth noting that the validity of the expansion (4) is doubtful for such a large value of ϵ . However, we will see below that this bifurcation occurs at a much smaller value of the pump if the dynamics of carriers is taken into account.

The stability with respect to long-wavelength spatial perturbations is determined by the two other roots, which are zero for $\mathbf{q} = \mathbf{0}$. For small \mathbf{q} they are approximated by a quadratic form

$$\text{Re}(\lambda) \approx \sum_{\substack{i=1 \\ j<i}}^2 \phi_{ij}(\epsilon) q_i q_j,$$

where $\phi_{ij}(\epsilon)$ are determined from an expansion of the characteristic polynomial into a series of ϵ . In order to establish the stability of the solutions of Eq. (10), it is sufficient to check the negative definiteness of this quadratic form. The analysis shows that for TW solutions (11) the negative definiteness condition leads to the following inequalities:

$$\phi_{11} = -4 \text{Re}(G_\alpha)^2 [\text{Re}(a_{11}^+ G_\alpha^*)] \epsilon + O(\epsilon^2) < 0, \quad (17)$$

$$\det(\phi_{ij}) = \phi_{11}\phi_{12} - \phi_{21}\phi_{22} = 2 \text{Re}(G_\alpha)^4 \{ -\text{Im}(a_{22}^+) \text{Im}(G_\alpha) [\text{Im}(a_{22}^+) \text{Im}(G_\alpha) + 2 \text{Re}(a_{22}^+) \text{Re}(G_\alpha)] + 16 \text{Im}(a_{11}^+) \text{Im}(G_\alpha) \text{Re}(a_{12}^+ G_\alpha^*) + \text{Re}(G_\alpha) [16 \text{Re}(a_{11}^+) \text{Re}(a_{12}^+ G_\alpha^*) - \text{Re}(G_\alpha) \text{Re}(a_{22}^+)^2] \} \epsilon^2 + O(\epsilon^3) > 0. \quad (18)$$

These conditions are met if the system is stable. For typical parameters of the laser cavity and values of α ($|\alpha| < 6$), the system of inequalities (17),(18) reduces to a single condition, $\alpha > \alpha_0$, where α_0 depends on the parameters of the cavity and usually is close to zero. For example, for the parameters used in [15], $\alpha_0 \approx -0.02$. Therefore, the TW solution (11) is absolutely stable at the threshold for $\alpha > \alpha_0$, and unstable with respect to long-wavelength perturbations for $\alpha < \alpha_0$. In the latter case, numerical simulations show that spatiotemporal chaos appears in the amplitude of the nonzero component of Eq. (11), whereas the other mode remains zero. For the original system (1),(2), this instability corresponds to a chaotic deformation of the TW.

It is important to note that at threshold $G_\alpha = \kappa(1 + i\alpha)G_{1\alpha}\mathcal{L}_\alpha/G_{0\alpha}$, where $G_{0\alpha}$, $G_{1\alpha}$, and \mathcal{L}_α are real quantities. The stability of TW and SW solutions, determined by Eqs. (13) and (14), depends only on α^2 . This means that the stability of the tilted wave with respect to perturbations with the same or the opposite wave vector does not depend on the sign of the α factor.

The stability in the case $\alpha = \alpha_0$, as well as in the case of usual isotropic reflectors, is not described by Eqs. (17),(18), because one or both of them become identical to zero. This means that derivatives of higher order have to be taken into account in Eqs. (6)–(10).

IV. TWO-MODE APPROXIMATION

Because the GL equations take into account only the static transverse carrier grating and do not include the dynamics of the carrier density, they cannot describe the system far above threshold. We recall that only the two field modes

$$e = e^{(+)} \exp(i\mathbf{k}_{\text{th}} \cdot \mathbf{x}_t) + e^{(-)} \exp(-i\mathbf{k}_{\text{th}} \cdot \mathbf{x}_t) \quad (19)$$

and the carrier modes

$$d = d^{(0)} + d^{(s)} \sin(2\mathbf{k}_{\text{th}} \cdot \mathbf{x}_t) + d^{(c)} \cos(2\mathbf{k}_{\text{th}} \cdot \mathbf{x}_t) = d^{(0)} + d^{(+)} \exp(2i\mathbf{k}_{\text{th}} \cdot \mathbf{x}_t) + d^{(-)} \exp(-2i\mathbf{k}_{\text{th}} \cdot \mathbf{x}_t) \quad (20)$$

were considered in the GL equations (10). Taking into account the temporal evolution of these carrier modes, we reduce the original system to differential equations for $e^{(+)}$, $e^{(-)}$, $d^{(0)}$, $d^{(c)}$, $d^{(s)}$ (or $d^{(+)}$, $d^{(-)}$). Because d is a real quantity, $d^{(+)}$, $d^{(-)}$ have to be complex conjugates and are not independent.

After substitution of Eqs. (19),(20) into Eqs. (1),(2), the following set of equations is obtained:

$$\dot{e}^{(+)} = (-L_\alpha + G_\alpha d^{(0)})e^{(+)} + G_\alpha d^{(+)}e^{(-)}, \quad (21)$$

$$\dot{e}^{(-)} = (-L_\alpha + G_\alpha d^{(0)})e^{(-)} + G_\alpha d^{(-)}e^{(+)}, \quad (22)$$

$$\begin{aligned} \dot{d}^{(0)} = & \mu - d^{(0)} - \mathcal{L}_\alpha d^{(c)} \text{Re}(e^{(-)}e^{(+)*}) \\ & - \mathcal{L}_\alpha d^{(s)} \text{Im}(e^{(-)}e^{(+)*}) - \mathcal{L}_\alpha d^{(0)} (|e^{(-)}|^2 + |e^{(+)}|^2), \end{aligned} \quad (23)$$

$$\begin{aligned} \dot{d}^{(c)} = & -d^{(c)} - \frac{1}{2} \mathcal{L}_\alpha [-d^{(c)} (|e^{(+)}|^2 + |e^{(-)}|^2) - \alpha d^{(s)} (|e^{(+)}|^2 \\ & - |e^{(-)}|^2)] - 2d^{(0)} \mathcal{L}_\alpha \text{Re}(e^{(-)}e^{(+)*}), \end{aligned} \quad (24)$$

$$\begin{aligned} \dot{d}^{(s)} = & -d^{(s)} - \frac{1}{2} \mathcal{L}_\alpha [-d^{(s)} (|e^{(+)}|^2 + |e^{(-)}|^2) - \alpha d^{(c)} (|e^{(-)}|^2 \\ & - |e^{(+)}|^2)] - 2d^{(0)} \mathcal{L}_\alpha \text{Im}(e^{(-)}e^{(+)*}). \end{aligned} \quad (25)$$

Because the carrier modes $d^{(i)}$ are functions only of time, this system does not describe the stability of SWs and TWs with respect to long-wavelength perturbations. However, it contains the stability with respect to temporal perturbations in the same set of modes.

Like Eq. (10), this system has two families of solution. The first is a TW,

$$d^{(c)} = d^{(s)} = 0, d^{(0)} = \mu_{\text{th}}, \quad (26)$$

$$|e^{(\pm)}|^2 = \frac{\mu - d^{(0)}}{\mathcal{L}_\alpha d^{(0)}}, \quad |e^{(\mp)}| = 0. \quad (27)$$

These are two one-parametric families of solutions each corresponding to a TW in a specific direction (+/-). In both families, the free parameter is the phase of the field.

The system (21)–(25) also has a two-parametric family of SW solutions with $|e^{(+)}| = |e^{(-)}|$. One of these is

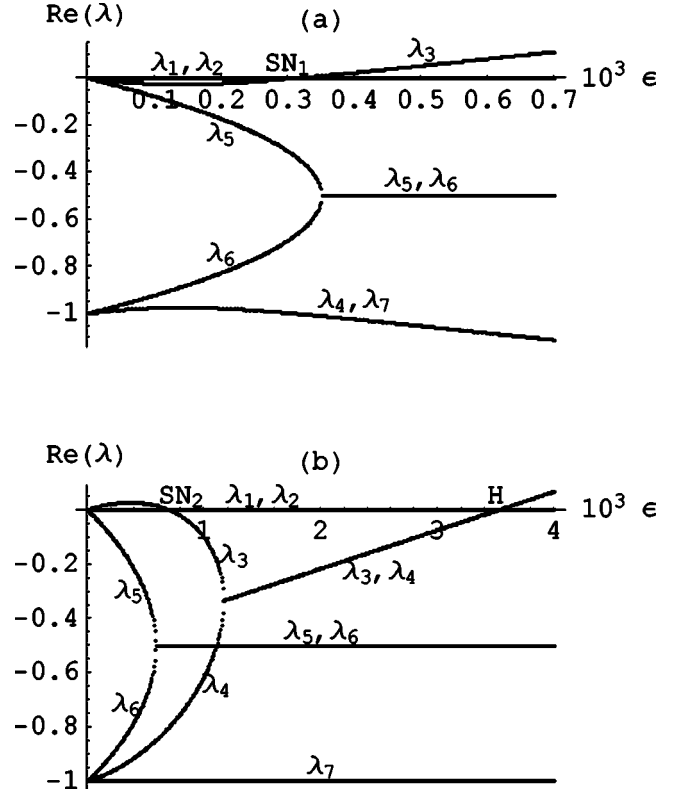


FIG. 2. The real parts of the roots of the characteristic polynomial of the system (21)–(25) for TWs (a) and SWs (b) in dependence on ϵ , the excess of the pump parameter above the first laser threshold. Different roots are marked by λ_i , where $i = 1 - 7$. Point SN_1 is the point of saddle-node bifurcation of TWs, SN_2 corresponds to a saddle-node bifurcation point of SWs, and H is the Hopf bifurcation point of SWs. The parameter values are as in Fig. 1. The value of ϵ is normalized to the threshold value of the pump parameter.

$$d^{(c)} = \frac{2[\text{Re}(L_\alpha) - \mu \text{Re}(G_\alpha)]}{3 \text{Re}(G_\alpha)}, \quad d^{(s)} = 0, \quad (28)$$

$$d^{(0)} = \frac{2 \text{Re}(L_\alpha) + \mu \text{Re}(G_\alpha)}{3 \text{Re}(G_\alpha)}, \quad (29)$$

$$e^{(+)} = e^{(-)} = \sqrt{\frac{\mu \text{Re}(G_\alpha) - \text{Re}(L_\alpha)}{3 \text{Re}(G_\alpha) \mathcal{L}_\alpha}}. \quad (30)$$

Here, the other members of this family can be obtained by either shifting the phase of the two fields by the same amount ϕ ,

$$e^{(+)} \rightarrow e^{(+)} \exp(i\phi), \quad e^{(-)} \rightarrow e^{(-)} \exp(i\phi), \quad (31)$$

or by phase shifts of opposite sign,

$$e^{(+)} \rightarrow e^{(+)} \exp(i\phi), \quad e^{(-)} \rightarrow e^{(-)} \exp(-i\phi). \quad (32)$$

In the case of the first transformation (31), all the variables except ϕ remain unchanged, whereas in the second case (32), they need to be changed appropriately. For example,

after rotation of the phase to an angle $\phi = \pi/2$ in Eq. (32), we obtain $d^{(c)} = 0$, $d^{(s)} \neq 0$, in contrast to Eq. (28).

Due to the existence of the above-mentioned families of solutions, the characteristic polynomial of the system (21)–(25), obtained by the stability analysis for both TW and SW solutions, has two zero roots λ_1, λ_2 . The real parts of all the roots, including zero ones, are shown in Fig. 2. Note that these roots (and therefore the system stability) do not depend on the sign of α . At a certain value of the pump parameter, the purely real eigenvalues (λ_5, λ_6 for both TW and SW solutions and λ_3, λ_4 for SW solutions only), which were initially corresponding to the field and carrier modes, merge and give rise to a pair of complex conjugated roots.

In the case of TWs, the real eigenvalue λ_3 has the maximum growth rate (apart from the marginal λ_1, λ_2 .) At some value of the pump it starts to increase and crosses the imaginary axis at the saddle-node point SN_1 . This leads to destabilization of the TW solution.

For the case of the SW solution, also the root λ_3 is the one determining the stability. It is initially larger than zero and the SW solution is unstable. At some value of the pump parameter, λ_3 decreases and crosses zero at the point SN_2 . This implies a stabilization of the SW solution. It will be shown below that as a rule $\epsilon(SN_1) < \epsilon(SN_2)$.

Therefore, in the region between points SN_2 and H a situation is encountered, which is not predicted by the GL equations (10): the TW is unstable, whereas the SW is stable. Unfortunately, we cannot say anything definitely about the stability of SWs with respect to long-wavelength perturbations from Eqs. (21)–(25). However, numerical simulations of the full system (1) and (2) show that secondary bifurcation predicted by Eqs. (21)–(25) indeed appears for any sign of α (but $\alpha \neq 0$). In contrast, long-wavelength instabilities can lead only to chaotic deformations of the basic regimes, described above. It is connected with the fact that the transverse Fourier spectrum of the solutions is limited to one or two spots near $\pm \mathbf{k}_{th}$, and long-wavelength perturbations cannot be developed enough to completely destabilize the system.

The next bifurcation of the system is a Hopf bifurcation of SWs, taking place at the point H , because two complex conjugated roots λ_3 and λ_4 cross the imaginary axis. Antiphase pulsations appear in the amplitudes of the field modes (Fig. 3). Close to the secondary bifurcation threshold, the oscillations are rather harmonic [Fig. 3(a)]. The modulation depth of the oscillations increases with increasing pump current. Further away from threshold and/or for high values of the α factor, the temporal shape of the oscillations is highly anharmonic, resembling a switchinglike dynamics between states in which one or the other TW is dominating [Fig. 3(b)].

In experiments, usually only time-averaged images are recorded. The pulsations in the TWs due to Hopf bifurcation cause a decrease of the contrast of averaged SWs (Fig. 4). The results of simulations of the initial system (1) and (2) and the reduced one (21)–(25) shown in this figure show the similarity of the dynamics of both systems. This proves again the main role of temporal instabilities predicted by Eqs.

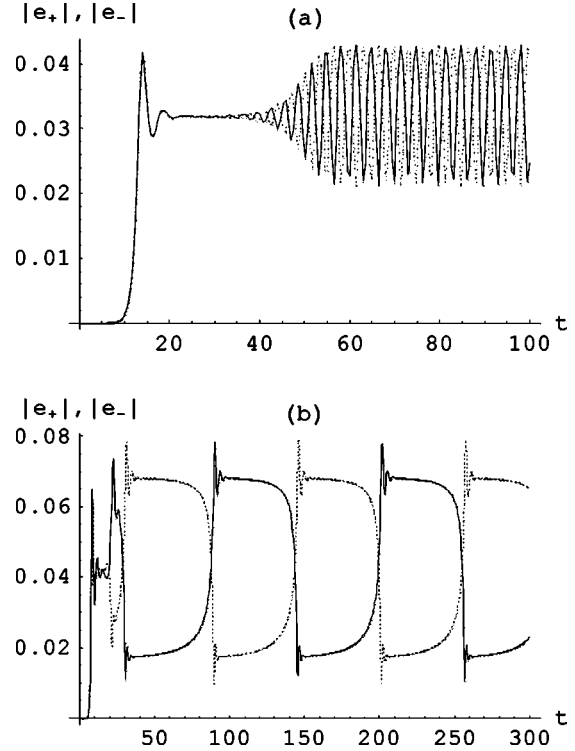


FIG. 3. The dynamics of the field amplitudes, corresponding to the wave traveling to the left (e^- , solid curve) and to the right (e^+ , dotted curve) after the Hopf bifurcation in SWs. The parameter values are marked on Fig. 5 by a circle (a) and rectangle (b). Time is normalized to T_1 (relaxation time of carriers). The initial conditions correspond to the laser being off.

(21)–(25). The contrast of the averaged pattern appearing in Eqs. (1) and (2) is slightly less because of spatial degrees of freedom.

The contrast tends to some value near zero, when the regime, shown in Fig. 3(b), appears.

The loss of stability of TWs and the stabilization of SWs may appear also in quintic GL equations, though for a level of pumping, which is different from the more accurate value

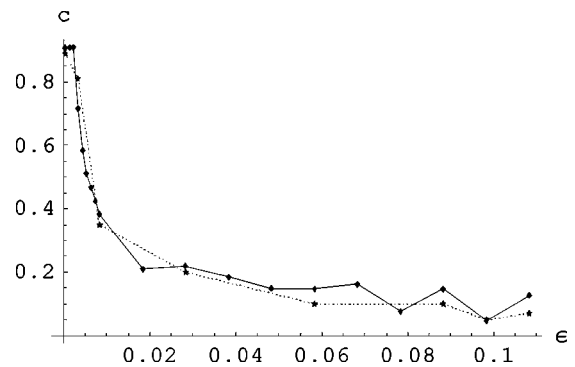


FIG. 4. The dependence of the contrast, $c = (|e_{max}| - |e_{min}|) / |e_{max}|$, of the time-averaged pattern on ϵ , the excess of the pump level above the first laser threshold. The solid curve is a result of simulations of the system (21)–(25), and the dotted one is a result of simulations of the initial system (1) and (2). The parameters are the same as in Fig. 2.

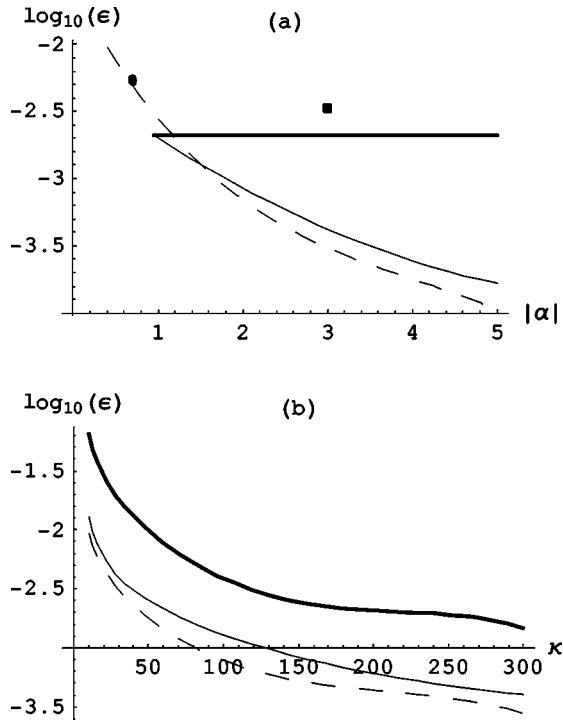


FIG. 5. The dependence of the bifurcation thresholds (see Fig. 2) SN_1 (dashed curve), SN_2 (solid curve), and H (bold solid curve) on the modulus of the α factor (a) and on the field decay rate κ (b). The excess of pump level above generation threshold is given in a logarithmic scale.

obtained from an analysis of Eqs. (21)–(25). In contrast, the Hopf bifurcation cannot appear in GL-like equations of any order without spatial derivatives, because of the following reasoning. Without the spatial derivatives, Eq. (10) is invariant with respect to separate phase shifts of each field. Due to this symmetry, the phase degrees of freedom can be removed from the GL equations (10) resulting in two real equations for the amplitudes of $e^{(\pm)}$. Because $|e^{(+)}| = |e^{(-)}|$ for a SW solution, the equations, linearized around the SW solution, are symmetric with respect to the replacement $\delta|e^{(+)}| \leftrightarrow \delta|e^{(-)}|$. Therefore, the linear evolution matrix of this system is real and symmetric. It is known that the eigenvalues of such a matrix are real (in the present case the dimension of the matrix is 2×2 , and this fact can be easily seen directly). This excludes the possibility of a Hopf bifurcation, since it requires complex eigenvalues. This symmetry is broken by the last terms in equations (21),(22), containing $d^{(\pm)}$. Therefore, the dynamics of the carrier spatial grating, created by the two counterpropagating waves and described by $d^{(\pm)}$, plays a fundamental role in the dynamics of the system.

However, the strength of destabilization of the field due to its interaction with the carrier grating decreases with decreasing value of α . The corresponding values of the pump parameter at which these secondary bifurcations take place tend to move towards infinity when $\alpha \rightarrow 0$. The dependence of the threshold values for all the bifurcations on α is shown in Fig. 5(a). It is worth noting that the destabilization of TWs takes place always at smaller values of pump than the stabilization

of SWs. In the region between these two bifurcations there is switchinglike dynamics between the two TWs similar to the one presented in Fig. 3(b).

As discussed above for TW and SW solutions of the GL equations (10) [cf. also to Eqs. (13)–(16)], the stability of the solutions of Eqs. (21)–(25) does not depend on the sign of the α factor, because Eqs. (21)–(25) include only the stability of tilted waves with respect to perturbations with the same or the opposite transverse wave vector.

For typical values of the field decay rate in VCSEL cavities ($\kappa \approx 10^2$), the threshold for the secondary bifurcations is very low, i.e., the secondary bifurcations appear very close to the first laser threshold. This makes their experimental observation very difficult. However, Fig. 5(b) shows that the threshold for the secondary bifurcations grows with decreasing κ . Such a decrease of κ can be achieved experimentally either by increasing the reflectivity of the mirrors, or by increasing the length of the cavity.

V. DISCUSSION AND CONCLUSION

In this paper, we have investigated the stability and secondary bifurcations of TW and SW solutions in the system (1),(2) describing a laser with a transversely anisotropic cavity. The spatio-temporal dynamics just above threshold were studied by GL equations (10) for two transverse Fourier modes of the field only. Further above threshold, the dynamics of the carriers needs to be taken into account yielding the system of Eqs. (21)–(25).

The stability analysis of Eq. (10) shows that at the first laser threshold the SW is always unstable, whereas TW can be stable or unstable. It is unstable with respect to long-wavelength transverse perturbations, if the linewidth enhancement factor $\alpha < \alpha_0$, with $\alpha_0 \neq 0$. We can compare these results with the situation in an edge-emitting semiconductor laser, which is extended only in one transverse dimension. Hence only two spatial field modes can appear at threshold, which makes the situation similar to the one in a two-dimensional VCSEL with transverse anisotropy. Order parameter equations for edge-emitting lasers were proposed in [12] and consist of a Swift-Hohenberg equation, coupled to a mean flow (CSH). The CSH in [12] can be considered as a special case of Eqs. (1) and (2) with $\hat{L} = 1$, $\hat{G} = \text{const}(1 + i\alpha)$, $\text{Re}(L_{11}^{(\pm)(11)}) = 0$. Also d is set to 1 in the third term of the equation for carrier (2). Thus, the analysis of GLE (10) (with $y = 0$ for the 1D case) describes the phase instabilities near threshold in 1D edge emitters with a special choice of a_i^{\pm} . The boundary of instabilities for the 1D case is given by Eq. (17) only, which leads to the condition $\alpha_0 = 0$ for this special case. This matches the results obtained earlier [12].

If there is in addition some mechanism for a dispersion of the losses with respect to \mathbf{k}_t (as in a VCSEL due to the dependence of the reflection coefficient of the Bragg mirrors on the transverse wave number), the value of $\partial^2 R(\mathbf{k}_t) / \partial k_x k_x$ is nonzero and therefore $\partial^2 G(\mathbf{k}_t) / \partial k_x k_x$ is also nonzero and depends on α . This leads to a dependence of a_{11} on α , and therefore to a small shift of the value of α_0 in Eq. (17).

The investigation of the temporal dynamics of Eqs. (21)–(25) shows that if $\alpha \neq 0$, a sequence of secondary bifurca-

tions appears in the system: destabilizing of TW, stabilizing of SW, and, at last, destabilizing of this SW through a Hopf bifurcation. The last bifurcation causes antiphase pulsations in the amplitude of the counterpropagating field components.

The key role in this sequence of bifurcations is played by the coupling between the field and the spatial grating induced in the carrier distribution. The coupling depends on the α factor, influencing the phase relations of the interactions of the field and the carrier grating. This mechanism is similar to the mechanism of the temporal instability arising in bidirectional lasers under the creation of a longitudinal grating of population inversion [22,23]. In the case of a transversely isotropic laser, the above-described bifurcations do not take place because they are shadowed by strong phase instabilities, which in this case are not hindered by the anisotropy of the Bragg mirror.

For $\alpha \neq 0$, these secondary bifurcations are the decisive ones and numerical simulations show that they appear independently on the sign of α , whereas the long-wavelength instabilities can lead to chaotic deformations of the solutions predicted by Eqs. (21)–(25). For very small excess of pump above threshold of generation, these chaotic deformations are described by Ginsburg-Landau equations (10). In the latter case, chaos appears only for $\alpha < \alpha_0$, in the amplitude of

TWs, whereas the amplitude of the second mode remains zero.

It should be noted that whereas usually $\alpha < 0$ for semiconductor materials, it was suggested to be taken as positive for quantum-well VCSEL in previous investigations [21] in order to describe an overall guiding, appearing in this kind of lasers due to temperature effects [21]. Further work is needed to investigate the combined action of carrier-induced anti-guiding and carrier-induced guiding due to the competing electronic and thermal nonlinearities.

It is obvious that the system (21)–(25) does not describe all instabilities in the system. For example, recent work shows that even in the case $\alpha = 0$ (for CO₂ laser) there can be secondary bifurcations [24], which leads to complex dynamical behavior by the excitation of many spatial modes. Therefore, additional investigations need to be carried out for a full characterization of the possible instabilities in the system considered here.

ACKNOWLEDGMENT

I.V.B. is grateful to the Deutsche Forschungsgemeinschaft for the financial support of his visit to Muenster.

-
- [1] K. Iga, F. Koyama, and S. Kinoshita, *IEEE J. Quantum Electron.* **24**, 1845 (1988).
 - [2] K.J. Ebeling, *SUSSP Proc.* **50**, 295 (1998).
 - [3] R. Michalzik, M. Grabherr, R. Jäger, M. Müller, and K.J. Ebeling, *Proc. SPIE* **3419**, 187 (1998).
 - [4] L.A. Lugiato, G.L. Oppo, J.R. Tredicce, L.M. Narducci, and M.A. Pernugo, *J. Opt. Soc. Am. B* **7**, 1019 (1990).
 - [5] P.K. Jakobsen, J.V. Moloney, A.C. Newell, and R. Indik, *Phys. Rev. A* **45**, 8129 (1992).
 - [6] P.K. Jakobsen, J. Lega, Q. Feng, M. Staley, J.V. Moloney, and A.C. Newell, *Phys. Rev. A* **49**, 4189 (1994).
 - [7] J. Lega, P.K. Jakobsen, J.V. Moloney, and A.C. Newell, *Phys. Rev. A* **49**, 4201 (1994).
 - [8] S.P. Hegarty, G. Huyet, J.G. McInerney, and K.D. Choquette, *Phys. Rev. Lett.* **82**, 1434 (1999).
 - [9] T. Ackemann, S. Barland, M. Cara, S. Balle, J.R. Tredicce, R. Jyager, M. Grabherr, M. Müller, and J.K. Ebeling, *J. Opt. B: Quantum Semiclassical Opt.* **2**, 406 (2000).
 - [10] A.C. Newell and J.V. Moloney, *Nonlinear Optics* (Addison-Wesley, Reading, MA, 1992).
 - [11] J. Lega, J.V. Moloney, and A.C. Newell, *Physica D* **83**, 478 (1995).
 - [12] J.V. Moloney, *J. Opt. B: Quantum Semiclassical Opt.* **1**, 183 (1999).
 - [13] N.A. Loiko and I.V. Babushkin, *Kvant. Electron* **31**, 221 (2000) [*Quantum Electron.* **31**, 221 (2000)].
 - [14] E.J. D'Angelo, E. Izaguirre, G.B. Mindlin, G. Huyet, L. Gil, and J.R. Tredicce, *Phys. Rev. Lett.* **68**, 3702 (1992).
 - [15] N.A. Loiko and I.V. Babushkin, *J. Opt. B: Quantum Semiclassical Opt.* **3**, S241 (2001).
 - [16] K.D. Choquette, K.L. Lear, R.P. Schneider, Jr., R.E. Leibenguth, J.J. Figiel, S.P. Kilcoyne, M. Hagerott-Crawford, and J.C. Zolper, *Proc. SPIE* **2382**, 125 (1995).
 - [17] J. Martin-Regalado, J.L.A. Cilla, and J.J. Rocca, *Appl. Phys. Lett.* **70**, 3350 (1997).
 - [18] M.P. van Exter, A.K. Jansen van Doorn, and J.P. Woerdman, *Phys. Rev. A* **56**, 845 (1997).
 - [19] A.K. Jansen van Doorn, M.P. van Exter, A.M. van der Lee, and J.P. Woerdman, *Phys. Rev. A* **55**, 1473 (1997).
 - [20] M.C. Cross and P.C. Hohenberg, *Rev. Mod. Phys.* **65**, 851 (1993).
 - [21] M. San Miguel, *SUSSP Proc.* **50**, 339 (1998).
 - [22] L.A. Kotomtseva, N.A. Loiko, and A.M. Samson, *J. Opt. Soc. Am. B* **2**, 232 (1985).
 - [23] Y. I. Khanin, *Principles of Laser Dynamics* (Elsevier, Amsterdam, 1995).
 - [24] F. Encinas-Sanz, I. Leyva, and J.M. Guerra, *Phys. Rev. A* **62**, 043821 (2000).
 - [25] D.J. Babic, Yo. Dagli, N. Chung, and J.E. Bowers, *IEEE J. Quantum Electron.* **29**, 1950 (1993).
 - [26] M. Born and E. Wolf, *Principles of Optics* (Pergamon, New York, 1980).